ACS APPLIED MATERIALS & INTERFACES

Research Article

www.acsami.org

A Mechanistic Explanation of the Peculiar Amphiphobic Properties of Hybrid Organic–Inorganic Coatings by Combining XPS Characterization and DFT Modeling

Alessandro Motta,*[,†] Oliviero Cannelli,[†] Alice Boccia,[†] Robertino Zanoni,*[,†] Mariarosa Raimondo,[‡] Aurora Caldarelli,[‡] and Federico Veronesi[‡]

[†]Dipartimento di Chimica, Università degli Studi di Roma "La Sapienza" and INSTM UdR Roma, piazzale Aldo Moro 5, I-00185, Roma, Italy

[‡]ISTEC CNR, Institute of Science and Technology for Ceramics, National Research Council, Via Granarolo, 64, 48018 Faenza, Italy

Supporting Information

ABSTRACT: We report a combined X-ray photoelectron spectroscopy and theoretical modeling analysis of hybrid functional coatings constituted by fluorinated alkylsilane monolayers covalently grafted on a nanostructured ceramic oxide (Al_2O_3) thin film deposited on aluminum alloy substrates. Such engineered surfaces, bearing hybrid coatings obtained via a classic sol–gel route, have been previously shown to possess amphiphobic behavior (superhydrophobicity plus oleophobicity) and excellent durability, even under simulated severe working environments. Starting from XPS, SEM, and contact angle results and analysis, and combining it with DFT results, the present investigation offers a first mechanistic explanation at a molecular level of the peculiar properties of the hybrid organic–inorganic coating in terms of composition and surface structural arrangements. Theoretical modeling shows that the active fluorinated moiety is strongly anchored on the alumina sites with single Si-O-Al bridges and that the residual valence of Si is saturated by Si–O–Si bonds which form a reticulation with two vicinal fluoroalkylsilanes. The resulting hybrid coating consists of stable rows of fluorinated alkyl chains in reciprocal contact, which form well-ordered and packed monolayers.

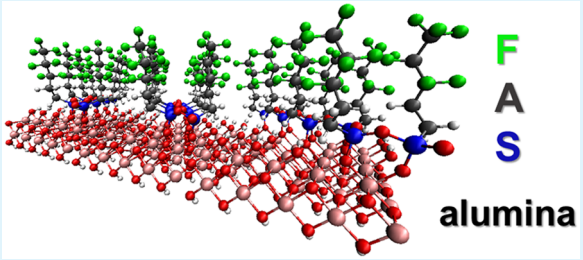

KEYWORDS: *amphiphobicity, superhydrophobicity, surface chemistry, X-ray photoelectron spectroscopy (XPS), density functional theory (DFT), hybrid organic–inorganic coatings, nanostructured alumina*

1. INTRODUCTION

Amphiphobicity[1] is the sum of hydrophobicity and oleophobicity, and is defined as the ability of a surface to repel both water and liquids with lower surface tension, e.g., oils and alkanes. Such ability is usually quantified in terms of contact angles that liquid droplets form on the surface. Amphiphobicity has a huge impact in the many fields where properties such as corrosion resistance, low friction, drag reduction, deicing are needed. A surface is, respectively, termed hydrophobic or superhydrophobic[2] when the associated water contact angles are larger than 90° or 150°, while it is oleophobic or superoleophobic if the above conditions are reached by employing a liquid of low surface tension. Superhydrophobicity can be generated by different methodologies,[3] among which we employed surface functionalization by inorganic or hybrid organic–inorganic thin films, produced as nanostructured deposits via sol–gel routes.[4] The water-based synthesis of superhydrophobic functional oxide layers thus obtained offers great advantages in terms of eco-compatibility, versatility, and future scaling-up with respect to the current solvent-based preparation. However, it is well-known that practical application of strongly water-repellent surfaces must overcome their mechanical fragility and poor durability.[5−9] Analogously, the synthesis of durable amphiphobic materials is still highly challenging. In a previous work,[4] we reported on the obtainment of amphiphobic surfaces characterized by surface energy values lower than 3 mN/m. Additionally, we demonstrated their outstanding repellence, durability, and chemical stability.[4] By way of a characterization of their wetting behavior, surface energy, and microstructure, we showed that nanostructured hybrid coatings deposited on aluminum withstand severe environments and mechanical stress without noticeable loss in their amphiphobicity. Such behavior makes these coated surfaces potentially antisticking materials with applications as self-cleaning, anti-icing, antifouling, and low-friction components. We present here a combined XPS, SEM, and theoretical investigation which aims at giving a mechanistic explanation of the peculiar amphiphobic properties of the hybrid organic–inorganic coating. While elegant literature reports have dealt with theoretical simulations of peculiar wetting properties such as the anti-icing properties of superhydrophobic alumina surfaces,[10] the superhydrophobic

Received: May 20, 2015
Accepted: August 26, 2015
Published: August 26, 2015

DOI: 10.1021/acsami.5b04376
ACS Appl. Mater. Interfaces 2015, 7, 19941−19947

properties of fatty acid adsorbed on iron oxides,[11] and the interface of superhydrophobic surfaces in contact with water,[12] we intend here to offer a combination of XPS measurements and DFT calculations to better understand the property/structure relationship of these materials at a molecular level.

2. EXPERIMENTAL DETAILS

2.1. Preparation of Amphiphobic Aluminum Alloy Surfaces. Alumina nanoparticles in the form of aqueous sols were prepared as follows: Ethyl acetoacetate (>99%, Sigma-Aldrich) was added to deionized water as chelating agent and mixed for a few minutes. At 70 °C, aluminum-tri-*sec*-butoxide (97%, Sigma-Aldrich) and nitric acid (0.5 M) to promote peptization were added in sequence. The reaction mixture was left under stirring at 70 °C for 24 h. The molar ratios of chelating agent, nitric acid, and total water with respect to the metal alkoxide were set to 1, 0.3, and 90, respectively. The pH of the as-prepared sol was 3.5. Particle size distribution of the alumina suspension, in terms of hydrodynamic diameter, was evaluated by dynamic light scattering (DLS) (DLS Zetasizer Nano S, Malvern Instrument) working in backscattering modus (2θ equal to 173°) at 25 °C. Average values corresponding to four different measurements were provided. Hydrodynamic diameter includes the coordination sphere and the species adsorbed on the particle surface such as stabilizers, surfactants, and so forth. DLS analysis also provides a polydispersion index (PDI, adim.), ranging from 0 to 1, whose value is related to the distribution of particle sizes in the colloidal suspension. The samples prepared in the present work showed a Gaussian-type particle size distribution with a PDI of 0.4 and an average particle size of 44 nm.

Sandblasted aluminum alloy (Al1050 99% H24) foils, with dimensions of 100 × 50 × 1.5 mm^3 and surface roughness R_a (measured by 3-D profilometer Talysurf CCI 3000) in the 4−5 μm range, have been considered as reference samples (sample A). After ultrasonication in ethanol for 5 min to remove impurities, Al foils were coated with the aqueous Al_2O_3 sol by dip-coating under the following conditions: dipping-withdrawing speed of 2 mm/s and residence time of 5 s. After drying at room temperature, coated samples were treated at 400 °C for 60 min, then boiled in distilled water for 30 min to form flaky bohemite, and thermally treated again at 400 °C for 10 min, getting the final transformation to γ-alumina (sample B). Finally, a solution of fluoroalkylsilanes (FAS) in 2-propanol solution (Dynasylan SIVO CLEAR EC, Evonik) without any further purification or dilution was dip-coated on the samples' surfaces (dipping withdrawing speed: 2 mm/s; residence time: 120 s), followed by consolidation at 150 °C for 30 min). By this procedure, aluminum foils with a hybrid organic/inorganic surface layer, characterized by an air-filled nanostructure, were produced (sample C).

Surface morphology of coated samples was investigated with a field emission scanning electron microscope (FESEM Gemini Columns SIGMA Zeiss), operating at 3 keV at a working distance of 3 mm, and collecting the images with the in-lens secondary electron detector. The thickness of the coatings was estimated by FESEM observations of cross-sectional images, being in the 200−400 nm range.

Full details of the experimental procedure and of the characterization of the samples are described in a previous work.[4]

2.2. Determination of Contact Angle and Surface Energy. Contact angle (CA) measurements with water (γ = 72.0 mN/m@20 °C) and hexadecane (γ = 27.5 mN/m@20 °C) were performed by an optical tensiometer equipped with a CCD camera (OCA 15 Plus, DataPhysic Instruments) by the sessile drop method (drop volume of 1 μL). For both liquids, CA values were obtained as the average of 10 measurements performed at ambient conditions (T = 22 ± 1°, RH = 50 ± 2%) on different points of the samples. The optical profiles of water and hexadecane droplets are given in Figure 1. Surface energy (SE) was calculated applying the Owens−Wendt−Kaelble model.[13]

2.3. XPS Measurements. XPS measurements were performed using a modified Omicron NanoTechnology MXPS system equipped with a monochromatic X-ray source (Omicron XM-1000), a dual X-ray anode (Omicron DAR 400), and an Omicron EA-127−7 energy analyzer. The experimental conditions adopted were: excitation by Al

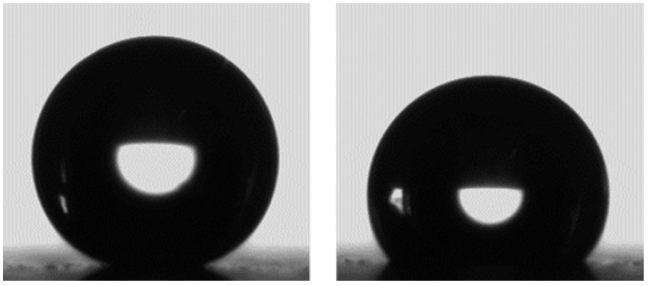

Figure 1. Optical profiles of (left) water and (right) hexadecane droplets.

Kα photons ($h\nu$ = 1486.7 eV) or Mg Kα photons ($h\nu$ = 1253.6 eV) both generated operating the anode at 14−15 kV, 10−20 mA. All the photoionization regions were acquired using an analyzer pass energy of 20 eV, except for the survey scan, which was taken at 50 eV pass energy. Take-off angles of 11° and 71° with respect to the sample surface normal were adopted. The measurements were performed at room temperature, and the base pressure in the analyzer chamber was about 2 × 10^{-9} mbar during the spectra detection. The binding energy (BE) of the Si $2p_{3/2}$ bulk component at 99.7 eV was used as an internal standard reference for the BE scale (accuracy of ±0.05 eV) for samples containing FAS. All measurements were conducted in the least possible time after sample preparation. The experimental spectra were theoretically reconstructed by fitting the peaks to symmetric Voigt functions and the background to a Shirley or a linear function. XPS atomic ratios (±10% associated error) between relevant core lines were obtained from experimentally determined area ratios corrected for the corresponding Wagner sensitivity factors.[14]

2.4. Computational Details. DFT-based calculations have been performed with the CP2K/Quickstep package, using a hybrid Gaussian and plane-wave method.[15] A double-quality plus polarization Gaussian basis set (DZVP) was employed for the Al atom, and a triple-quality plus polarization Gaussian basis set (TZVP) was employed for all the other atoms. The Goedecker−Teter−Hutter pseudopotentials[16] together with a 400 Ry plane-wave cutoff were used to expand the densities obtained with the Perdew−Burke−Ernzerhof (PBE)[17] exchange-correlation density functional. Dispersion forces are taken into account using the Grimme DFT-D3Method.[18] Only the Γ point was considered in a supercell approach. Periodic boundary conditions were applied in all directions of space. Gibbs free energy values were evaluated for a simplified cluster model by performing geometry optimization, followed by the frequency calculation, implemented as a module in the Gaussian09 code.[19] Translational, rotational, and vibrational entropy contributions were evaluated for the fluoroalkylsilane condensation on a AlO_6H_9 cluster. Entropic corrections were appended to the energy profile evaluated on the 2D system using the CP2K code. Gaussian09 calculations were performed at the level of the B3LYP formalism. The standard all-electron 6-31G** basis was used for all atoms.[20]

2.5. Surface Model. It is assumed that the nanostructured alumina surface is covered by a terminal oxy-hydroxide thin layer whose degree of hydration depends on the external conditions. In air, this layer is often identified as pseudoboehmite.[21] For this reason, the alumina surface was modeled by the boehmite (AlOOH) phase. This is a layered compound exposing (100), (010), (001), and (101) faces, with different ratios. The surface stability increases with the coordination numbers of Al and hydroxyl groups, and the most stable is the basal (010) surface, which exhibits saturated coordinated Al ions and bridging OH groups and is characterized by low surface energy and low chemical reactivity.[22] We chose to investigate the (010) surface as the most stable and representative face (Figure 2).

The (010)-terminated slab modeled in the present study consists of two OH-terminated AlOOH layers. It was constructed starting from the bulk cell structure optimized without dispersion contributions (for which the cell parameters are a = 2.89 Å, b = 12.09 Å, c = 3.74 Å, in good agreement with experimental values of a = 2.87 Å, b = 12.23 Å, c

DOI: 10.1021/acsami.5b04376
ACS Appl. Mater. Interfaces 2015, 7, 19941−19947

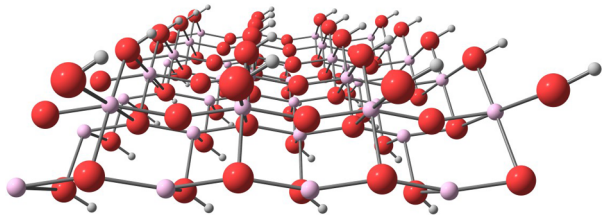

Figure 2. Modeled boehmite (010) surface used in this study.

= 3.69 Å).[23] Then, we chose a (4 × 5) supercell of a boehmite surface (14.452 × 14.976 Å), with an empty space of 15 Å in the *z* direction perpendicular to the surface. The bottom-side OH groups were frozen to take into account bulk constraints.

3. RESULTS AND DISCUSSION

3.1. Repellence against Liquids and Surface Energy. The as-prepared aluminum alloy sample (sample A) presents contact angles of about 96° and 4° with water (WCA) and hexadecane (HCA), respectively (Table 1), indicating a moderate hydrophobicity and a high wettability with hexadecane. The presence of the nanostructured Al_2O_3 layer in sample B—whose typical flower-like structure and thickness are shown in Figure 3—involves, as expected, a complete surface affinity to water (superhydrophilicity, WCA < 5°).

Table 1. Static Contact Angle with Water (WCA) and Hexadecane (HCA) and Surface Energy of the Reported Samples

sample	WCA (deg)	HCA (deg)	SE (mN/m)
A	95.8 ± 3.1	4.0 ± 1.1	28.2
B	<5.0 ± 1.0	n.d.	80.9
C	179.7 ± 0.2	141.8 ± 6.2	0.50

Further functionalization with FAS molecules (sample C) proved to be crucial in changing the surface into superhydrophobic (WCA of 179.7°) and oleophobic (HCA of 141.8°). In the overall sequence of surface modifications A → C, the surface energy (SE) values are significantly lower, maximizing the gap between SE and the alkane surface tension (Table 1).

3.2. XPS Results. XPS analysis was conducted on samples representing the full sequence of the surface functionalization process. Table 2 shows the relative surface atomic composition at each step of the sequence leading to the overlayer formation.

Table 2. XPS Surface Atomic Composition Relative to Al

sample	O/Al	C/Al	F/Al	Si/Al
A	3.7	5.2	0.18	0.21
B	3.0	1.5	0.13	
C	6.3	23	34	2.3

An overlayer of boehmite (AlOOH) is expected to terminate the clean, air-exposed aluminum alloy sample (sample A), with a chemical state for the Al intermediate between totally oxidized (Al_2O_3) and totally hydroxylized [$Al(OH)_3$]. The corresponding O/Al ratio shows an excess of oxygen with respect to the characteristic boehmite stoichiometry (O/Al = 2.0), due to the oxygen-containing carbonaceous species arising from contamination. The O 1s peak cannot be reliably analyzed in terms of components because of its large and symmetric line shape (Figure S4). However, a correction to the O/Al atomic ratio for sample A can be obtained from curve-fitting of the composite C 1s peak, where three main components can be found (Figure 4, left). They are, respectively, assigned to the aliphatic backbone (284.9 eV) and to species containing C-O (286.1 eV) or C(O)O (289.0 eV) groups,[24] the latter two components representing 22% and 5% of the total area. By taking into account the above data, a contribution to the O/Al atomic ratio of 1.7 can be subtracted from the 3.7 value reported in Table 1. (details of the calculations may be found in the Supporting Information). This analysis gives a value of 2.0 for the O/Al atomic ratio for sample A, as expected for the boehmite stoichiometry.

XPS wide range spectrum of sample A (Figure S1) reveals the presence of a trace of Si, which is a minor alloy component, and of F, likely a contaminant.

The formation of a nanostructured alumina layer on sample B does not modify the atomic composition at the surface. In fact, an AlOOH layer is still expected at the topmost surface. The oxygen amount is in excess with respect to the characteristic boehmite stoichiometry, as found for sample A. By applying the same procedure reported above for sample A (see the Supporting Information), we obtained a value of 2.2 for the O/Al atomic ratio of sample B, after correction for the contribution due to surface contamination.

After the step of treatment with FAS, the surface undergoes a drastic change. Oxygen, carbon, silicon, and fluorine highly increase as a consequence of FAS anchoring to the surface. A dependence of the F/C ratio on the exposure time under X-rays was noticed, with a relevant change in the C 1s line shape with time. In order to acquire a less perturbed C 1s spectrum,

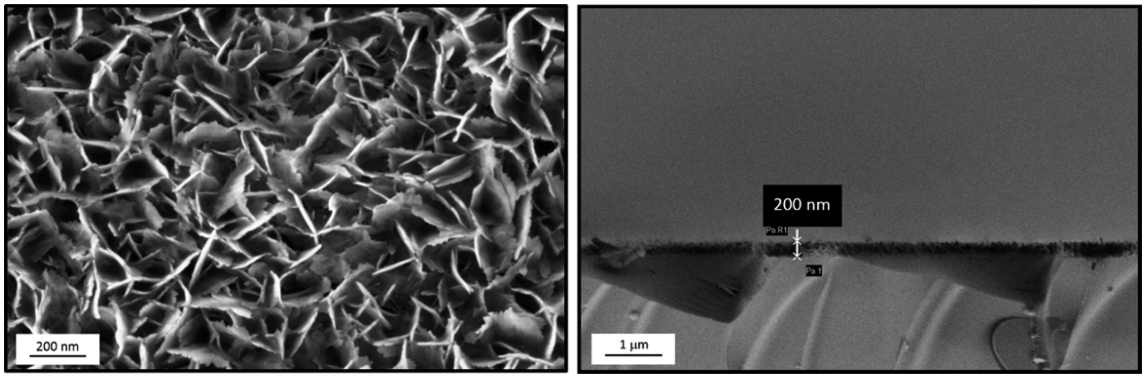

Figure 3. FESEM images: (Left) The characteristic *flower-like* surface morphology. (Right) Thickness generated after Al_2O_3 sol deposition.

DOI: 10.1021/acsami.5b04376
ACS Appl. Mater. Interfaces 2015, 7, 19941−19947

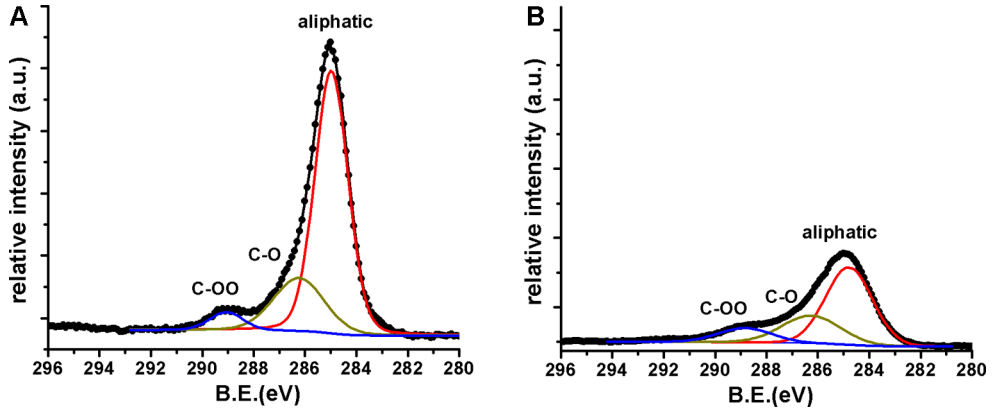

Figure 4. XPS C 1s region of sample A (left), and sample B (right). Peak intensities are normalized to the relative amount of Al.

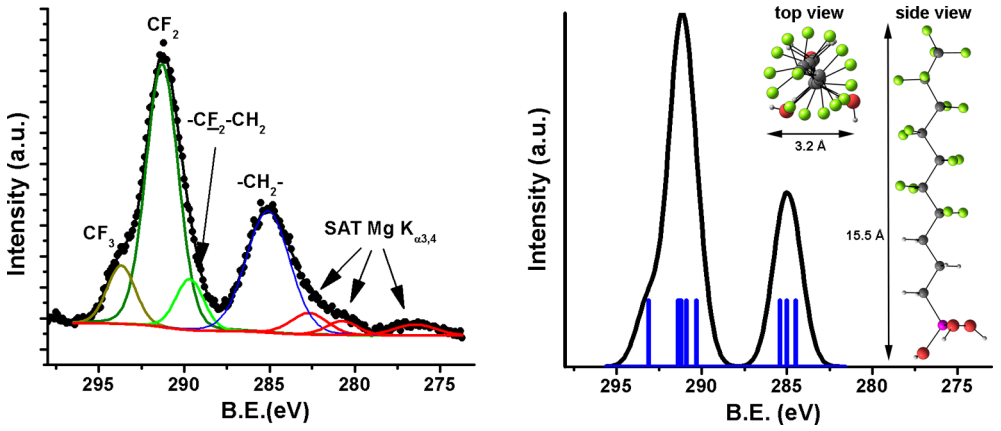

Figure 5. (Left) XPS C 1s region of sample C. (Right) Gaussian convolution of C 1s orbital energies computed for the model molecule $CF_3(CF_2)_6(CH_2)_3Si(OH)_3$.

this region was acquired within the shortest possible time (~5 min). The experimentally determined relative amounts of C, F, and Si allow us to verify the length of the alkyl chain effectively present at the surface, and its degree of fluorination. On the basis of the values of XPS C/Si ratio (10) and F/C ratio (1.45), the alkyl chain can be associated with a sequence of 10 carbon atoms, 7 of which are perfluorinated.

Two main composite signals are present in the C 1s region. The C-F and the alkyl chain components are found on the high and low binding energy side, respectively. A detailed curve-fitting analysis (Figure 5, left) shows that the C-F signal can be theoretically reconstructed with three main components assigned to terminal $\underline{C}F_3$-CF_2– at 293.7 eV, –$\underline{C}F_2$-CF_2– at 291.3 eV, and –$\underline{C}F_2$-CH_2– at 289.7 eV.[24]

The large component under the alkyl signal (fwhm = 3.0 eV) centered at 285.0 eV includes the following molecular components: –CF_2-$\underline{C}H_2$–, the bulky alkyl chain (–$\underline{C}H_2$–), and –$\underline{C}H_2$-Si–.[24] For a satisfactory curve-fitting, the satellite peaks of the most intense C-F components, excited by Mg $K\alpha_{3,4}$, are also added in the theoretical reconstruction. The relative intensity ratios between the above components allow us to obtain the molecular identity of the FAS present at the surface. In particular, a 1:1 ratio is found between the terminal CF_3 and the –$\underline{C}F_2$-CH_2– species, as expected, a 1:5 ratio between the CF_3 and –CF_2– components, and a 1:3 between CF_3 with the alkyl signal. All of these data hint at a molecular formula CF_3–$(CF_2)_6$-$(CH_2)_3$-SiR_3, which should be considered as the experimentally determined averaged formula reflecting the overall effects of preparation steps and exposure to X-ray photons and to a high vacuum. The obtained structure, in which a short alkyl chain is present between SiR_3 and the fluorinated long chain, is likely to allow for a better packing of the silane molecules on the surface, due to the smaller size of H compared to F atoms. A totally perfluorinated chain would prevent formation of the monolayer on the surface. We further investigated this point by means of DFT calculations.

3.3. DFT Results. DFT investigations have been performed to understand at a molecular level the grafting mechanism of FAS on the surface. Molecular calculations on the above proposed FAS molecule have been performed, and the simulated XPS spectrum is shown on the right side of Figure 5. The plotted curve is based on the Gaussian convolution of the core electron energy of the experimentally determined FAS molecule present at the surface (Koopmans' theorem). A satisfactory linear correlation (R^2 = 0.98) was found between the C 1s core electron orbital and the experimental XPS peak components assigned to the FAS molecule. The perfect match of the corrected curve obtained by the linear relationship with the experimental values confirms the structure deduced by XPS analysis. The optimized structure of the hydrolyzed FAS molecule, reported in the inset of Figure 5, shows a helical arrangement of the fluorinated chain due to steric interactions among vicinal CF_2 groups. This model further suggests a maximum stable thickness of one monolayer (15.5 Å) on the alumina surface.

DOI: 10.1021/acsami.5b04376
ACS Appl. Mater. Interfaces 2015, 7, 19941–19947

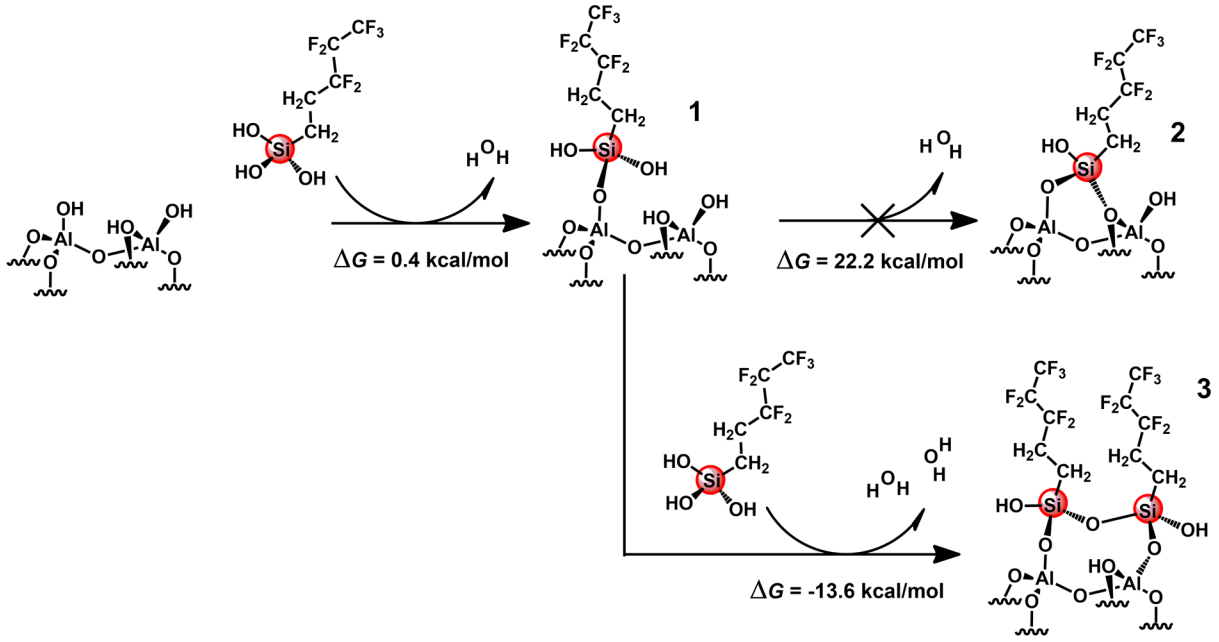

Figure 6. Condensation mechanism of FAS molecules on an alumina surface.

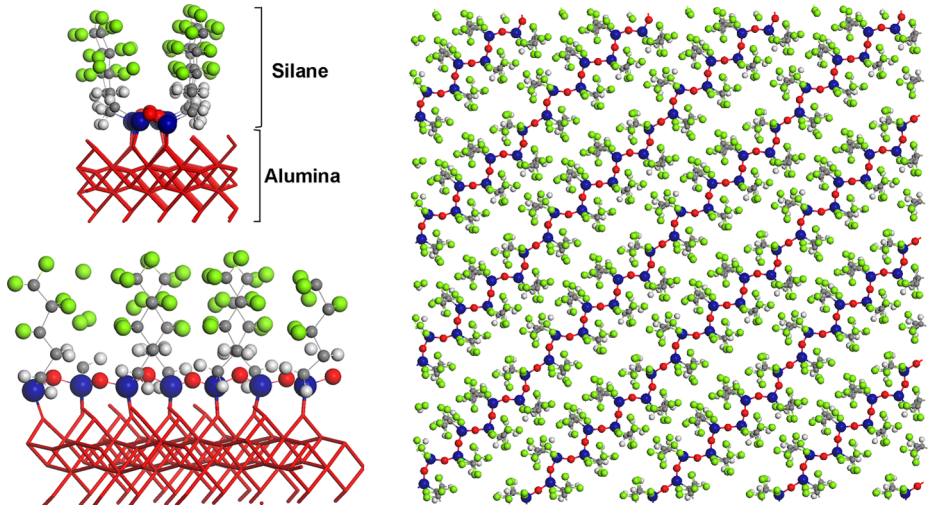

Figure 7. (Left) Side views of a single silane row grafted on the alumina surface. C in gray, Si in blue, O in red, F in green. (Right) Top wide view of the silane rows, forming a monolayer on the alumina surface. The underlying boehmite structure is omitted for clarity.

It is well-known that fluoroalkylsiloxanes possess a dual behavior, with one end reacting with surface atoms and the other possessing nonwetting termination, represented by a CF_3 group. Structural and energetic analysis was conducted on the condensation process between a fluoroalkylsiloxane prototypical model compound $[CF_3(CF_2)_2(CH_2)_2Si(OH)_3]$ and the alumina surface hydroxyl groups. In principle, silane can react with three hydroxyl groups at the surface. The first condensation reaction (structure **1** in Figure 6) was found to be isoergonic (ΔG = 0.4 kcal/mol).

Once the silane is anchored on the surface, a second condensation reaction between the Si-OH terminal group and a hydroxyl group of the alumina surface can occur (structure **2** in Figure 6). This reaction is entropically driven, since one further water molecule is released from the surface, but it is also very enthalpically disfavored, probably because of the geometrical mismatch between the Si−OH distance of the silane (2.7 Å) and the corresponding distance in the surface hydroxyl groups (2.9 Å). In fact, the overall energetic balance between entropic and enthalpic contributions is 22.2 kcal/mol, and this path can be considered not viable. It is worth noting that, once a monodentate anchoring of the silane occurs, two other reactive OH groups remain available at the silane molecule for further intermolecular condensations.

We found that the condensation of a second silane molecule in a vicinal surface hydroxyl group and the parallel condensation between the two silane molecules releasing two further water molecules (structure **3** in Figure 6) is a very favorable process (ΔG = −14 kcal/mol). In this case, the double condensation process is driven by an entropic contribution due to formation of two water molecules (one particle becoming anchored, two particles being released). It is expected that the formation of infinite silane chains grafted on the surface will be a spontaneous process because of both the mentioned entropic gains. Figure 7 shows the surface arrangement of the silane chains. It can be seen that a zigzag

DOI: 10.1021/acsami.5b04376
ACS Appl. Mater. Interfaces 2015, 7, 19941−19947

configuration of the condensed silane molecules occurs, producing a double fluoroalkyl row for each silane chain (Figure 7, left). Moreover, the grafted silane chains are in contact with each other, covering the entire surface and, in turn, producing a monolayer (Figure 7, right). Further contribution of the dispersion forces are, then, to be considered among the vicinal silane chains on the same row and vicinal silane chains belonging to vicinal rows. It was found that the formation of a monolayer of condensed silane rows is associated with a ΔG of −33 kcal/mol, which is, in turn, strongly favored.

Once a monolayer is formed, only 40% of the hydroxyl surface groups react with FAS, because of the steric hindrance of the silane molecules that, in turn, do not allow for an interaction of the FAS molecules with all of the hydroxyl groups at the surface, as experimentally evidenced.[25] Moreover, steric interaction among the FAS molecules induces a preferentially linear arrangement of the fluoroalkyl chains, with the terminal CF_3 group pointing away from the surface, along a perpendicular direction (Figure 7, left). This result is consistent with previous XANES characterization of FAS monolayers anchored on various substrates.[26] The thickness of the monolayer can be estimated as 1.5 nm from the computed optimized structure of FAS, as shown in the inset of Figure 5. The grafted silane chains are well-ordered and in contact each other (Figure 7, right), producing a well-packed monolayer on the surface, which can explain the peculiar properties of the FAS-treated surfaces. Further calculations have been performed to assess the effects of the alkyl portion of the overall FAS chain on the monolayer stability. Using a totally perfluorinated silane model molecule $[CF_3(CF_2)_4Si(OH)_3]$, monolayer formation is strongly disfavored (ΔG = 52 kcal/mol) as a consequence of the larger steric encumbrance of $-CF_2-$ groups compared to $-CH_2-$ groups. The crucial role of the purely alkyl part of the FAS carbon chain is clearly disclosed.

4. CONCLUSIONS

Amphiphobic hybrid monolayers on aluminum substrates have been investigated by a combination of XPS and SEM measurements with DFT modeling. The nature of the Al substrate after coating with nanostructured alumina and the characteristics of the partially fluorinated alkylsilane anchored on the surface were explored by XPS, and disclosed in terms of chemical composition and atomic ratios. DFT modeling highlighted the anchoring mechanism and the preferred monolayer arrangement at the surface. The ensemble of experimental and theoretical results hints at polymerized silane rows well-ordered and packed as the structural motif formed by FAS bound to the alumina surface. According to DFT results, the silane units are covalently anchored through single Si-O-Al bridges. The two additional hydroxyl groups bound to Si in FAS remain available for condensation with additional interacting silane molecules, which favors the formation of polymeric rows. These findings may help achieve a deeper comprehension of the peculiar properties of amphiphobic hybrid coatings.

ASSOCIATED CONTENT

Supporting Information

The Supporting Information is available free of charge on the ACS Publications website at DOI: 10.1021/acsami.5b04376.

XPS wide spectra of samples A, B, and C; XPS C 1s, Al 2p, and O 1s regions of samples A, B, and C; and XPS F 1s region of sample C (PDF)

AUTHOR INFORMATION

Corresponding Authors

*E-mail: alessandro.motta@uniroma1.it (A.M.).
*E-mail: robertino.zanoni@uniroma1.it (R.Z.).

Notes

The authors declare no competing financial interest.

ACKNOWLEDGMENTS

Computational resources supporting this work were provided by the CINECA award N. HP10CBHAYD 2015 under the ISCRA initiative (A.M.).

REFERENCES

(1) Lu, Y.; Sathasivam, S.; Song, J.; Crick, C. R.; Carmalt, C. J.; Parkin, I. P. Robust Self-Cleaning Surfaces that Function when Exposed to either Air or Oil. *Science* **2015**, *347*, 1132−1135.
(2) Erbil, H. Y.; Demirel, A. L.; Avci, Y.; Mert, O. Transformation of a Simple Plastic into a Superhydrophobic Surface. *Science* **2003**, *299*, 1377−1380.
(3) Yan, Y.; Gao, N.; Barthlott, W. Mimicking Natural Superhydrophobic Surfaces and Grasping the Wetting Process: A Review on Recent Progress in Preparing Superhydrophobic Surfaces. *Adv. Colloid Interface Sci.* **2011**, *169*, 80−105.
(4) Raimondo, M.; Blosi, M.; Caldarelli, A.; Guarini, G.; Veronesi, F. Wetting Behavior and Remarkable Durability of Amphiphobic Aluminum Alloys Surfaces in a Wide Range of Environmental Conditions. *Chem. Eng. J.* **2014**, *258*, 101−109.
(5) Verho, T.; Bower, C.; Andrew, P.; Franssila, S.; Ikkala, O.; Ras, R. H. A. Mechanically Durable Superhydrophobic Surfaces. *Adv. Mater.* **2011**, *23*, 673−678.
(6) Liu, J.; Huang, W.; Xing, Y.; Li, R.; Dai, J. Preparation of Durable Superhydrophobic Surface by Sol−Gel Method with Water Glass and Citric Acid. *J. Sol-Gel Sci. Technol.* **2011**, *58*, 18−23.
(7) Zhu, X.; Zhang, Z.; Men, X.; Yang, J.; Wang, K.; Xu, X.; Zhou, X.; Xue, Q. Robust Superhydrophobic Surfaces with Mechanical Durability and Easy Repairability. *J. Mater. Chem.* **2011**, *21*, 15793−15797.
(8) Ishizaki, T.; Masuda, Y.; Sakamoto, M. Corrosion Resistance and Durability of Superhydrophobic Surface Formed on Magnesium Alloy Coated with Nanostructured Cerium Oxide Film and Fluoroalkylsilane Molecules in Corrosive NaCl Aqueous Solution. *Langmuir* **2011**, *27*, 4780−4788.
(9) She, Z.; Li, Q.; Wang, Z.; Li, L.; Chen, F.; Zhou, J. Researching the Fabrication of Anticorrosion Superhydrophobic Surface on Magnesium Alloy and its Mechanical Stability and Durability. *Chem. Eng. J.* **2013**, *228*, 415−424.
(10) Ruan, M.; Hou, H.; Li, W.; Wang, B. Theoretical Study of the Adsorption/Dissociation Reactions of Formic Acid on the α-Al_2O_3(0001) Surface. *J. Phys. Chem. C* **2014**, *118*, 20889−20898.
(11) Chernyshova, I. V.; Ponnurangam, S.; Somasundaran, P. Adsorption of Fatty Acids on Iron (Hydr)oxides from Aqueous Solutions. *Langmuir* **2011**, *27*, 10007−10018.
(12) Doshi, D. A.; Shah, P. B.; Singh, S.; Branson, E. D.; Malanoski, A. P.; Watkins, E. B.; Majewski, J.; van Swol, F.; Brinker, C. J. Investigating the Interface of Superhydrophobic Surfaces in Contact with Water. *Langmuir* **2005**, *21*, 7805−7811.
(13) Owens, D. K.; Wendt, R. C. Estimation of the Surface Free Energy of Polymers. *J. Appl. Polym. Sci.* **1969**, *13*, 1741−1747.
(14) Wagner, C. D.; Davis, L. E.; Zeller, M. V.; Taylor, J. A.; Raymond, R. H.; Gale, L. H. Empirical Atomic Sensitivity Factors for Quantitative Analysis by Electron Spectroscopy for Chemical Analysis. *Surf. Interface Anal.* **1981**, *3*, 211−225.

DOI: 10.1021/acsami.5b04376
ACS Appl. Mater. Interfaces 2015, 7, 19941−19947

(15) The CP2K developers group: http://www.cp2k.org (accessed July 30, 2015).
(16) Goedecker, S.; Teter, M.; Hutter, J. Separable Dual-Space Gaussian Pseudopotentials. *Phys. Rev. B: Condens. Matter Mater. Phys.* **1996**, *54*, 1703−1710.
(17) Perdew, J. P.; Burke, K.; Ernzerhof, M. Generalized Gradient Approximation Made Simple. *Phys. Rev. Lett.* **1996**, *77*, 3865−3868.
(18) Grimme, S. J.; Antony, J.; Ehrlich, S.; Krieg, H. A Consistent and Accurate Ab Initio Parametrization of Density Functional Dispersion Correction (DFT-D) for the 94 Elements H-Pu. *J. Chem. Phys.* **2010**, *132*, 154104.
(19) Frisch, M. J.; Trucks, G. W.; Schlegel, H. B.; Scuseria, G. E.; Robb, M. A.; Cheeseman, J. R.; Scalmani, G.; Barone, V.; Mennucci, B.; Petersson, G. A.; Nakatsuji, H.; Caricato, M.; Li, X.; Hratchian, H. P.; Izmaylov, A. F.; Bloino, J.; Zheng, G.; Sonnenberg, J. L.; Hada, M.; Ehara, M.; Toyota, K.; Fukuda, R.; Hasegawa, J.; Ishida, M.; Nakajima, T.; Honda, Y.; Kitao, O.; Nakai, H.; Vreven, T.; Montgomery, J. A., Jr.; Peralta, J. E.; Ogliaro, F.; Bearpark, M.; Heyd, J. J.; Brothers, E.; Kudin, K. N.; Staroverov, V. N.; Kobayashi, R.; Normand, J.; Raghavachari, K.; Rendell, A.; Burant, J. C.; Iyengar, S. S.; Tomasi, J.; Cossi, M.; Rega, N.; Millam, J. M.; Klene, M.; Knox, J. E.; Cross, J. B.; Bakken, V.; Adamo, C.; Jaramillo, J.; Gomperts, R.; Stratmann, R. E.; Yazyev, O.; Austin, A. J.; Cammi, R.; Pomelli, C.; Ochterski, J. W.; Martin, R. L.; Morokuma, K.; Zakrzewski, V. G.; Voth, G. A.; Salvador, P.; Dannenberg, J. J.; Dapprich, S.; Daniels, A. D.; Farkas, Ö.; Foresman, J. B.; Ortiz, J. V.; Cioslowski, J.; Fox, D. J. *Gaussian 09*, Revision D.01; Gaussian, Inc.: Wallingford, CT, 2009.
(20) Francl, M. M.; Pietro, W. J.; Hehre, W. J.; Binkley, J. S.; Gordon, M. S.; Defrees, D. J.; Pople, J. A. Self-Consistent Molecular Orbital Methods. XXIII. A Polarization-Type Basis Set for Second-Row Elements. *J. Chem. Phys.* **1982**, *77*, 3654.
(21) van den Brand, J.; Blajiev, O.; Beentjes, P. C. J.; Terryn, H.; de Wit, J. H. W. Interaction of Anhydride and Carboxylic Acid Compounds with Aluminum Oxide Surfaces Studied Using Infrared Reflection Absorption Spectroscopy. *Langmuir* **2004**, *20*, 6308−6317.
(22) Jonsson, E. O.; Thygesen, K. S.; Ulstrup, J.; Jacobsen, K. W. Ab Initio Calculations of the Electronic Properties of Polypyridine Transition Metal Complexes and Their Adsorption on Metal Surfaces in the Presence of Solvent and Counterions. *J. Phys. Chem. B* **2011**, *115*, 9410−9416.
(23) Corbato, C. E.; Tettenhorst, R. T.; Cristoph, G. G. Structure Refinement of Deuterated Boehmite. *Clays Clay Miner.* **1985**, *33*, 71−75.
(24) Beamson, G.; Briggs, D. *High Resolution XPS of Organic Polymers: The Scienta ESCA300 Database*; John Wiley & Sons: Chichester, U.K., 1992.
(25) Saleema, N.; Sarkar, D. K.; Gallant, D.; Paynter, R. W.; Chen, X.-G. Chemical Nature of Superhydrophobic Aluminum Alloy Surfaces Produced via a One-Step Process Using Fluoroalkyl-Silane in a Base Medium. *ACS Appl. Mater. Interfaces* **2011**, *3*, 4775−4781.
(26) Schondelmaier, D.; Cramm, S.; Klingeler, R.; Morenzin, J.; Zilkens, Ch.; Eberhardt, W. Orientation and Self-Assembly of Hydrophobic Fluoroalkylsilanes. *Langmuir* **2002**, *18*, 6242−6245.

DOI: 10.1021/acsami.5b04376
ACS Appl. Mater. Interfaces 2015, 7, 19941−19947